844.6 NM PHOTOMETER CALIBRATION FOR GROUND-BASED THERMOSPHERIC OXYGEN DENSITY MEASUREMENT

By

Dawn Haken

Senior Thesis in Electrical Engineering

University of Illinois at Urbana-Champaign

Advisor: Professor Lara Waldrop

May 2019

Abstract

Ground-based observations of spectral emission lines are commonly used to investigate conditions in the upper atmosphere, where in-situ measurements are generally infeasible. The atomic oxygen 844.6 nm emission line is a prominent feature in the midlatitude thermosphere. Energetic photoelectron flux, radiative recombination of O^+ ions, and active radio-frequency heating are known to generate 844.6 nm emission. The 844.6 nm emission line has both well-understood photochemistry and line brightness sensitivity to oxygen density. These characteristics make it a favorable candidate for oxygen density measurement in the upper thermosphere. Previously, 844.6 nm observations have been made using high resolution spectrometry and tilting filter photomultiplier tubes. However, these efforts lacked spatial data as well as absolute intensity calibration required to derive oxygen density. This thesis presents the design, calibration, and first light observations of a novel imaging photometer. The photometer will be capable of on-sky brightness calibration during routine observations from a ground-based facility. Absolute calibration of emission line brightness will advance current understanding of O 844.6 nm emission excitation sources and allow for oxygen density measurement.

Subject Keywords: atmospheric remote sensing; photometry; oxygen

Contents

1 Introduction

Atoms and molecules comprising gaseous atmospheres undergo numerous interactions which cause them to emit light in characteristic spectral patterns. Remote sensing of the spectral distribution of these so-called "airglow" emissions is a common means of estimating atmospheric conditions such as winds and temperatures at high altitudes, where direct *in situ* sensing is prohibitively difficult. Estimation of atmospheric properties such as composition or species abundance from measurements of airglow emission line brightness, rather than spectral line shape, is more challenging and thus less commonly used. Not only does accurate interpretation of measured emission brightness require complete knowledge of the photochemical processes responsible for generating the observed emission, but also the processes themselves must be sensitive to changes in the parameter under investigation. Few airglow emission lines generated in the Earth's upper atmosphere meet these requirements.

Atomic oxygen (O) emission at 844.6 nm has long been considered an exception. Its relatively simple photochemistry and bright twilight signature makes it a potentially ideal candidate for remote sensing of O density in the upper thermosphere near low Earth orbit (100 - 400km). Although total mass density in this region is well known from copious satellite drag data, knowledge of the neutral composition comprising that total is notoriously poor. As the most abundant thermospheric species, O governs both energy and momentum transfer with the ionosphere [1]. A new means of remotely sensing O density based on 844.6 nm emission inversion would provide crucial data for advancing assimilative models and for validating physics-based understanding of the coupled atmospheric regions.

The O 844.6 nm emission is known to be generated in the mid-latitude thermosphere through impact between ground-state O atoms and energetic photoelectrons (PEs) [2], which are themselves created via natural solar photoionization (or active radio-frequency heating) of the neutral atmosphere. Knowledge of the incident electron flux would allow for estimation of the unknown O density from calibrated 844.6 nm emission brightness data as described in Section 2.1.1, provided that no other excitation mechanisms contribute to the observed emission. Recently, however, Waldrop et al. [3] has shown evidence that radiative recombination of O+ ions can be a non-negligible source of 844.6 nm excitation, though the climatological dependence of its significance relative to PE-impact is not known.

This thesis describes the optical design, calibration, and operation of a novel ground-based photometer for routine O 844.6 nm emission measurement and consequent O density sensing. The photometer is comprised of two channels, each with a narrowband filter and CCD imager, on a steerable alt-azimuth mount. The "off-band" background channel is subtracted from the "on-band" emission line channel. On-band filter wavelength calibration is carried out in a laboratory setting with an oxygen spectrum tube. On-sky calibration of atmospheric extinction is achieved through imaging stellar sources during observation campaigns.

2 Background

2.1 844.6 nm Emission Photochemistry

Electrons transitioning from the $(2p^3 3p)^3P$ state to the $(2p^3 s)^3S$ state in atomic oxygen emit the characteristic 844.6 nm triplet line, as shown in Figure 1. Members of the triplet are located at 844.638 nm, 844.676 nm, and 844.626 nm, in descending 5:3:1 intensity [4]. This transition occurs as part of radiative cascades from the highest atomic oxygen energy levels; significant energy is required for its excitation from ground state. Observations are typically restricted to twilight and night, due to the overwhelming solar continuum background in daylight. The 844.6 nm line is also observed in the aurora, where it is excited from auroral electron impact on O, as well as during high-power radio frequency (RF) heating of the atmosphere. At mid-latitudes, i.e., locations along closed geomagnetic field lines with magnetic dip angles greater than ~20°, two natural processes dominate 844.6 nm emission generation: PE impact on O and radiative recombination of O+ ions.

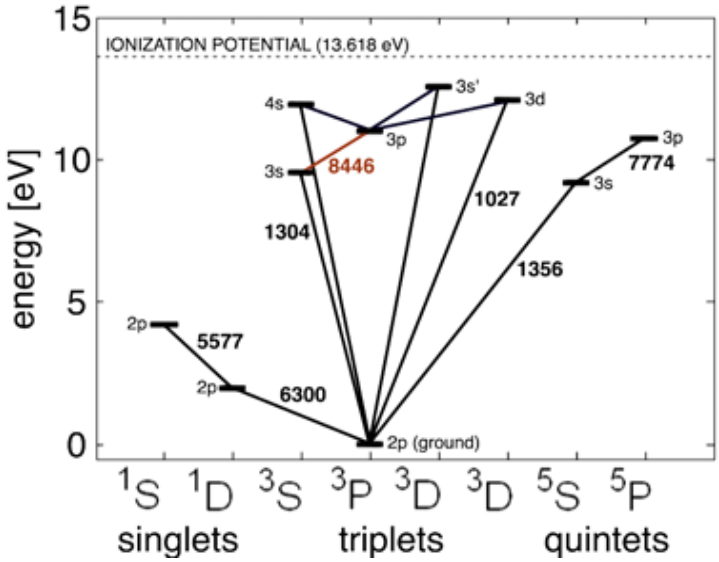

Figure 1: Partial Grotian diagram of atomic oxygen, where the 8446 Å transition highlighted.

2.1.1 Energetic electron impact

Photoelectron (PE) impact on oxygen atoms has long been believed to be the primary source of O 844.6 emission at mid-latitudes [2]. These high-energy PEs originate from solar photoionization of other atoms in the thermosphere. PEs are generated both locally and within the geomagnetically conjugate hemisphere, i.e. locations within the thermosphere at the opposite end of the local magnetic field line. A percentage of the PEs generated at the conjugate location travel along the magnetic field line and impact atomic oxygen in the local thermosphere. Typical sunset intensities of 844.6 nm emission are 50-100 R, dropping to 0 R as the PE flux diminishes with increasing solar zenith angle and thus height of the solid Earth shadow in the local atmosphere [2]. The relationship between atomic oxygen density and 844.6 nm radiance is an integration along instrument line of sight, as follows:

$$I(t) = \frac{4\pi}{10^6} \int_{los} ds\, [O](z) \int_E \sigma(E)\, \phi(E,z,t)\, dE \qquad (1)$$

where $I(t)$ is the time-dependent radiance in Rayleighs (defined as 10^6 photons/cm^2/sr/s), $[O]$ is the altitude z dependent atomic oxygen density, σ is the effective cross section for excitation of the upper 3p3P level of 844.6 nm transition, and ϕ is the energy E, altitude, and time-dependent PE flux.

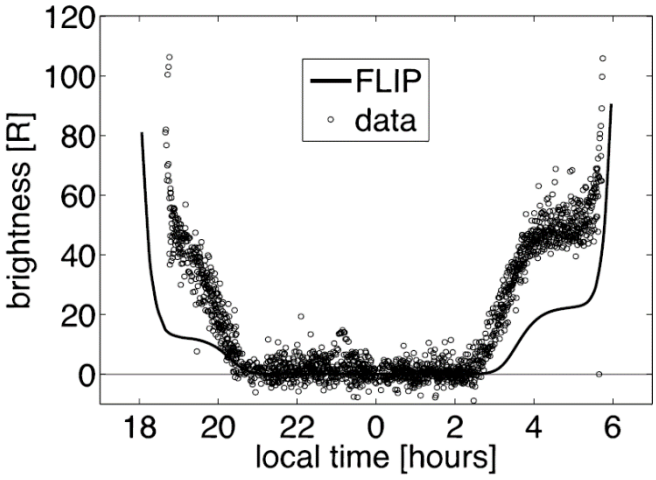

Figure 2: 844.6nm emission data and FLIP PE model calculations, winter at Arecibo Observatory, 1999 – 2002 [2].

Photoelectron flux is dependent on both local time and time of year. Local sunset and geomagnetic conjugate sunset occur at different times depending on the season. When the local atmosphere is dark and the conjugate atmosphere illuminated, 844.6 nm flux is observed as PEs from the conjugate location excite local oxygen. PE flux from the local and geomagnetic conjugate locations can be calculated by the physics-based Field Line Interhemispheric Plasma (FLIP) model, developed by P. Richards and D. Torr [5] [6]. Predicted 844.6 nm radiance is derived from the predicted flux, as per equation 1. Figure 2 shows a comparison of typical radiance data and FLIP model predictions. The FLIP model predicts the shape of the brightness curve, but underestimates the brightness. The historical data lacks absolute calibration, and the model may have systematic errors. Calibrated 844.6 nm measurements are needed to minimize these errors and allow for accurate estimation of [O] from data-model comparisons.

2.1.2 Radiative Recombination

Radiative recombination (RR) of O+ ions has been observed as a source of 844.6 nm emission at mid-latitudes [g] [3]. 844.6 nm radiance in Rayleighs is calculated as follows:

$$I = \frac{4\pi}{10^6} \int N_e(z)\, [O^+(z)]\, \alpha\big(T_e(z)\big)\, dz$$

where N_e is the altitude dependent electron density, $[O^+]$ is the O^+ density, and $\alpha(T_e)$ is the effective recombination coefficient, which is a function of altitude-dependent electron temperature T_e. With

accurate recombination coefficients, the contribution to measured 844.6 nm emission arising from radiative recombination can be estimated using coincident measurements of ionospheric parameters, such as from incoherent scatter radar facilities. Subtracting the estimated RR component from the total observed enables the PE-impact emission to be isolated for accurate [O] estimation. Radiative recombination emission, when present, is strongest in the twilight and decreases to near-zero at sunrise. It is more prominent during periods of increased solar and geomagnetic activity [3]. Absolutely calibrated measurements are needed to reduce uncertainty in the effective recombination coefficient derived from observed radiative recombination emission.

3 Instrument

The instrument consists of two photometer channels, and “on-band” and an “off-band”. Both channels use thin film interference filters and CCD imagers. The on-band filter is very narrow and designed to center on the 844.6 nm triplet at 25 °C. The off-band filter is centered at a nearby wavelength with no perceptible atmospheric emission lines. Off-band signals are treated as spectral background contamination and subtracted from the on-band signals. Instrument properties are summarized in Table 3.1, Table 3.2, and Table 3.3.

Figure 3: The two-channel photometer.

3.1 Optical Path

The two photometers which make up the instrument are identical aside from their filters. Both are f/5 systems, equipped with filter heaters, temperature control, and ATIK 490EX CCD cameras. The photometers are mounted side by side on an iOptron CubePro 8408 mount. This computerized AltAzimuth mount includes a GPS and ASCOM computer control.

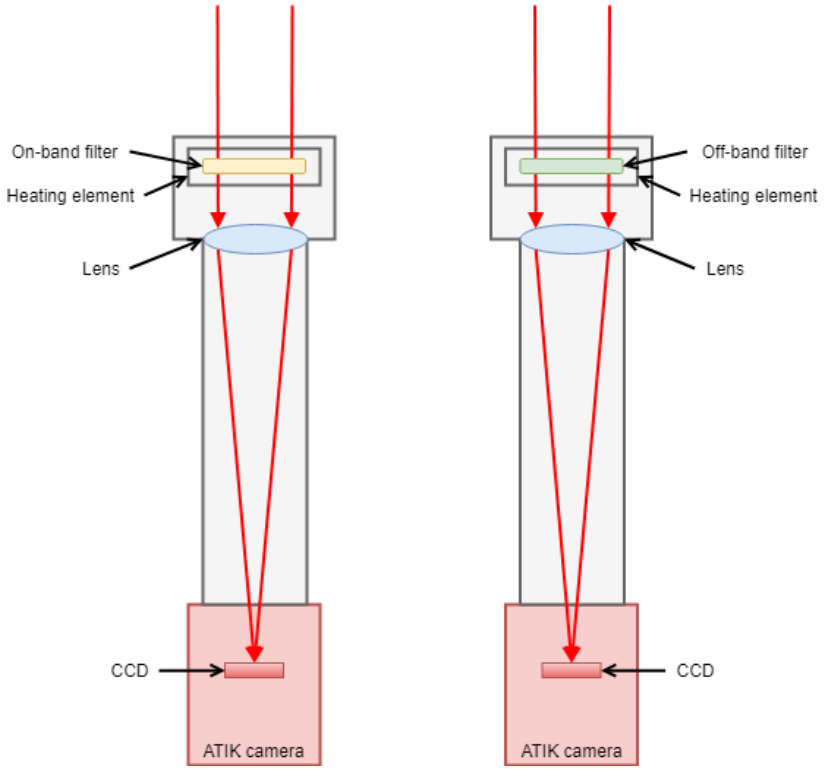

Figure 4: Optical path of the photometers.

3.2 Filters

Both the on-band and off-band filters are narrowband thin-film interference filters manufactured by the Andover Corporation. They are fixed such that the angle of incidence is 0°. The on-band filter was designed to have a center wavelength of 844.8 at 25 °C, which is blueshifted back to 844.6 due to the system's f/5 cone angle. The filter was chosen to be very narrow (~0.28 nm) to exclude nearby bright OH emission lines. The off-band filter's center wavelength is chosen to be nearby the target emission, but excluding any atmospheric emission lines. For both filters, the center wavelength shifts approximately 0.1 nm / 3.5 °C toward the red as its temperature increases.

3.3 Specification Tables

Table 3.1, Table 3.2, and Table 3.3 present a detailed overview of the instrument specifications.

Table 3.1: General Specifications

Characteristic	**Value**
CCD field of view (FOV)	172 arcmin x 138 arcmin
Pixel size	3.04 arcsec or 2.1696 x10^{-10} steradians
Focal length	250 mm
Aperture	50 mm
f/#	f/5

Table 3.2: Filter Specifications

Characteristic	On-band filter	Off-band filter
Center wavelength	844.80 nm	848.01 nm
Peak transmission	44.58%	50.20%
FWHM	0.282 nm	0.283 nm
Corresponding ATIK camera serial number	11901-141	11830-139

Table 3.3: Camera Specifications

Characteristic	Value
Sensor	SONY ICX814ALG
Resolution	3380 x 2704
Pixel size (µm)	3.69 x 3.69
Peak QE	71%
QE at 844.6 nm	26%
Readout noise (typical)	5e-
Dark current	~0.0003 electrons/ second at -10°
Gain factor	0.19e- / ADU

3.4 Operating Modes

The photometer has several operating modes, intended to carry out different functionalities. In every mode, the images downloaded from the cameras are saved as individual FITS files with relevant observation data in the header. The Pointing Calibration mode must be run before any of the other modes can produce useful results.

3.4.1 Pointing Calibration

In the pointing calibration mode, the mount's pointing is calibrated, and the star detection threshold is verified. The user manually moves the mount such that the photometers are pointing toward the zenith and the power distribution block is facing due south. Once the mount is in this position, the zero position is set. The user must execute the two-star alignment procedure in using the EQMOD software or hand controller. A star from the calibration catalog which is visible is selected, and the mount attempts to slew to the star. A 20-second exposure of the FOV is taken by one camera. The image is displayed rotated such that it appears upright. A star detection operation is applied to the image, and any potential stars are identified image. If no star is visible, the user must adjust the mount and take another image. The user must manually adjust the mount pointing to center the calibration star in the image, and then continue with the alignment procedure. This process is repeated for the second alignment star.

Once the two-star alignment is complete, the mount is slewed to a third star. If the star is within the FOV of the camera, the alignment has been successful, and imaging can proceed. If the third target star is not within the FOV, the alignment must be cleared and repeated. Once this third star has been successfully imaged, the difference in its location between the two photometer images is used to calculate the offset of the photometers.

3.4.2 On-Sky Intensity Calibration

The On-sky Intensity Calibration mode can be combined with either of the following imaging modes. When this mode is enabled, the photometer will periodically slew to a selected calibration star and image it. The exposure time for the star is based on the calibration sources catalog. The time between calibrations is selected by the user. Once calibration images have been downloaded, the images are automatically processed with the star detection function to verify that at least one star is within the field of view, and that the star is not overexposed. If no stars are detected, the cause is likely an obstructed FOV or a large pointing error. If the star is overexposed, another image is taken with a reduced exposure time.

3.4.3 Zenith Imaging

Zenith Imaging mode is used to gather airglow data at the zenith. In this mode, sky tracking is disabled and the photometer continuously images the local zenith. The target altitude and azimuth defaults to the zenith, but any altitude/azimuth coordinates can be chosen, such that the photometer can image in an arbitrary direction.

3.4.4 Single Field Line Imaging

In the Single Field Line Imaging mode, the photometer points along the local magnetic field line. The GPS coordinates from the mount are used to calculate the magnetic declination and dip angle from the World Magnetic Model (WWM). Magnetic declination describes the angle of the local magnetic field from true north. Dip angle describes the angle at which the local magnetic field "enters" Earth's surface. Since the observation is made "back" along the magnetic field line, the direction of observation is calculated as follows:

$$AZ = D + 180°$$

$$ALT = -I$$

where *AZ* is the azimuth angle in degrees, *D* is the magnetic declination, *ALT* is the altitude angle in degrees, and *I* is the magnetic dip angle. In single field line imaging mode, sky tracking is disabled. Images are taken continuously with both channels of the photometer.

3.5 Data Quality

Once images are collected from both channels of the photometer, hot pixels are subtracted, and the total counts for the entire image are summed. The signal for a given photometer channel can be calculated as follows:

$$S = \frac{\phi \eta t}{g} \tag{1}$$

where *S* is the signal value in ADU, ϕ is the flux, η is the quantum efficiency, *t* is the integration time, and *g* is the gain factor. The signal-to-noise ratio (SNR) for a given photometer measurement accounts for Poisson noise, dark current, and readout noise, and is calculated as follows:

$$SNR = \frac{S}{\sqrt{S + N_d t + {N_R}^2}} \tag{2}$$

where S is the signal, N_d is the dark noise, t is the integration time, and N_R is the readout noise. For the target observation, the 844.6 nm signal is calculated by subtracting the off-band background from the on-band measurement. The SNR for this combined measurement is

$$SNR = \frac{S_{on-band} - S_{off-band}}{S_{on-band} + S_{off-band} + 2N_d t + 2{N_R}^2} \tag{3}$$

Approximate dark noise and readout noise are given by the CCD manufacturer and can be found in Table 3.3.

Figure 5 presents predicted SNR values, given the 844.6 nm radiance in Rayleighs, and the off-band radiance as a percentage of the on-band radiance. Approximate off-band radiance percentages are derived from Waldrop et al, 2018 [3]. The background radiance decreases significantly overnight, as the 844.6 nm emission approaches zero. Integration times under 30 seconds will prevent any noticeable frame rotation due to the alt-azimuth configuration of the mount, regardless of the pointing direction.

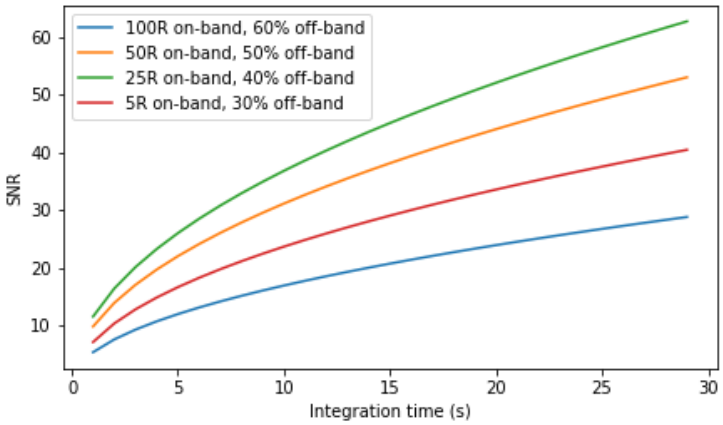

Figure 5: Predicted SNR values, given on-band radiance.

4 Absolute Intensity Calibration

The measured radiance depends both on instrument characteristics and on atmospheric extinction. The sensitivity of the instrument is dependent on the filter transmission, quantum efficiency, and gain value, values which each have their own uncertainties. Measured radiance is also dependent on atmospheric extinction, governed primarily by aerosol scattering, and thus airmass. Airmass is derived from flux measurements of a calibration star at a variety of altitudes throughout the night. The difference between measured flux and known flux from stellar spectral data can be used to derive the airmass at a given instrument look angle.

4.1 Filter Wavelength Calibration

Calibration of the on-band filter center wavelength is critical to the overall instrument calibration. In order to verify the temperature at which the filter is centered at the 844.6 nm emission, the relative signal from a calibrated source is measured for a range of temperatures. The temperature which corresponds to the peak signal is considered to be the operational temperature for the on-band filter. As a preliminary test, the on-band and off-band photometers were used to image an oxygen spectrum tube, which showed significant signal in the on-band a very little signal in the off-band.

4.2 On-Sky Airmass Calibration

During observation campaigns, calibration stars are used to find the atmospheric extinction of the 844.6 nm emission line. Multiple observations are made of the same star at varying altitudes is derived from a comparison of measured stellar flux and known flux from stellar spectra.

5 Data Pre-Processing

The two photometers are not exactly aligned with one another; the offset of the two photometers for a given observing session is known from the alignment procedure in Section 3.4.1. If there are stars which are visible in one channel but not in the other, they could introduce significant error. Therefore, the overlapping area of the two channels is analyzed, while the outside area is discarded. Approximately 90% of the area is expected to overlap. For both the on-band and off-band images, hot pixels are subtracted from the image, and the entire image is binned, resulting in a single value for the on-band and off-band channels. The off-band background is then subtracted from the on-band signal measurement.

5.1 Calibration Stars

The flux of the calibration source is measured using aperture photometry. The chosen calibration stars are very bright compared to neighboring stars; the calibration star is generally the only detectable star in the image. There is negligible overlap with the profiles of other stars, so de-blending techniques are not required, and aperture photometry suffices. A standard aperture radius is defined and centered on the calibration star in the image. The pixel values within this aperture are summed. An annulus is defined around the aperture, and the median value within this annulus is calculated. The median value is multiplied by the number of pixels within the aperture, resulting in the background sum. The background sum is subtracted from the aperture sum, and the result of is a flux value in ADU. This process is repeated for both the on-band and off-band calibration images.

6 Future Work

A calibrated oxygen source in a laboratory environment should be used to find the exact operational temperature of the on-band filter. An astronomical source which emits at 844.6 nm should also be observed as verification. The Orion Nebula has been extensive studied, and Cosmovici et al. present absolute fluxes for a number of positions in the nebula [7]. This mapping can be used as a calibration verification for the instrument. Once these further calibration processes are completed, the instrument can begin scientific observation campaigns.

7 Conclusion

The 844.6 nm atomic oxygen emission line has long been considered a candidate for remote sensing of neutral atomic oxygen density in the thermosphere. Its photochemistry is well understood and oxygen density is directly related to the emission line brightness. This thesis presents the design and control of a ground-based 844.6 nm imaging photometer. The steerable, two-channel design allows for on-sky intensity calibration during observation campaigns. Preliminary data pre-processing and data quality analysis showed that the instrument will meet its objectives. Calibrated brightness measurements of 844.6 nm airglow will contribute to better models of photochemical processes and the derivation of oxygen density in the thermosphere. [8]

References

[1] P. P. Joshi, L. S. Waldrop and C. G. M. Brum, "Ionospheric O+ momentum balance through charge exchange with thermospheric O atoms," *Journal of Geophysical Research: Space Phsycis,* vol. 123, pp. 9743-9761, 2018.

[2] L. S. Waldrop, R. Kerr and P. Richards, "Photoelectron impact excitation of OI 8446 Å emission observed from Arecibo Observatory," *Journal of Geophysical Research,* vol. 113, 2008.

[3] L. Waldrop, R. B. Kerr and Y. Huang, "Evidence for radiative recombination of O+ ions as a significant source of O 844.6 nm emission excitation," *Journal of Geophysical Research: Space Physics,* vol. 123, pp. 3078-3086, 2018.

[4] R. S. Lancaster, L. S. Waldrop, R. B. Kerr, J. Noto, S. C. Solomon, C. A. Tepley, R. Garcia and J. Friedman, "Brightness measurements of the nighttime O I 8446 Å airglow emission from the Millstone Hill and Arecibo Observatories," *Journal of Geophysical Research: Space Physics,* vol. 105, no. A3, pp. 5275-5290, 2000.

[5] P. G. Richards and D. G. Torr, "Ratios of photoelectron to EUV ionization rates for aeronomic calculations," *Journal of Geophysical Research,* vol. 99, pp. 8981-8992, 1988.

[6] P. G. Richards, "Seasonal and solar cycle variations of the ionospheric peak electron density: Comparison of measurement and models," *Journal of Geophysical Research,* vol. 106, pp. 12803-12820, 2001.

[7] C. B. Cosmovici, H. Olthof, F. Strafella, C. Barbieri, G. Canton and E. D'Anna, "Orion Nebula: Fabry-Perot high resolution OI (8446 Å) mapping," *Astronomy and Astrophysics,* vol. 72, pp. 241-245, 1979.

[8] T. G. Slanger, P. C. Cosby and D. L. Huestis, "Oxygen atom Rydberg emission in the equatorial ionosphere from radiative recombination," *Journal of Geophysical Research,* vol. 109, no. A10309, 2004.

Appendix A: Required Software

Table A.1: Operational software for the photometer

Software	Purpose	Source
Windows 10	Operating System	N/A
Python 3.7	Scripting language	https://www.anaconda.com/distribution/ (recommended)
ASCOM Platform 6.4	Instrument communications standard	https://ascom-standards.org/
EQMOD	Manual mount control and alignment, hand controller alternative	http://eq-mod.sourceforge.net/introindex.html
iOptron Commander and ASCOM Driver	Mount driver	https://www.ioptron.com/Articles.asp?ID=295
ATIK Core Software with Atik Cameras ASCOM camera driver	Camera driver	https://www.atik-cameras.com/downloads/
Python scripts	Operating modes and data pre-processing	https://gitlab.engr.illinois.edu/haken2/rapid-photometer